

# Linear and Nonlinear 3D-QSAR Approaches in Tandem with Ligand-Based Homology Modeling as a Computational Strategy To Depict the Pyrazolo-Triazolo-Pyrimidine Antagonists Binding Site of the Human Adenosine A<sub>2A</sub> Receptor

Lisa Michielan,<sup>†</sup> Magdalena Bacilieri,<sup>†</sup> Andrea Schiesaro,<sup>†</sup> Chiara Bolcato,<sup>‡</sup> Giorgia Pastorin,<sup>‡</sup> Giampiero Spalluto,<sup>\*,‡</sup> Barbara Cacciari,<sup>§</sup> Karl Norbet Klotz,<sup>||</sup> Chosei Kaseda,<sup>⊥</sup> and Stefano Moro<sup>\*,†</sup>

Molecular Modeling Section, Dipartimento di Scienze Farmaceutiche, Università di Padova, via Marzolo 5, I-35131 Padova, Italy, Dipartimento di Scienze Farmaceutiche, Università di Trieste, Piazzale Europa 1, I-34127 Trieste, Italy, Dipartimento di Scienze Farmaceutiche, Università degli Studi di Ferrara, Via Fossato di Mortara 17-19, I-44100 Ferrara, Italy, Institut für Pharmakologie, Universität of Würzburg, D-97078 Würzburg, Germany, and Yamatake Corporation, 1-12-2 Kawana, Fujisawa-shi Kanagawa 251-8522, Japan

Received August 10, 2007

The integration of ligand- and structure-based strategies might sensitively increase the success of drug discovery process. We have recently described the application of Molecular Electrostatic Potential autocorrelated vectors (*autoMEPs*) in generating both linear (Partial Least-Square, PLS) and nonlinear (Response Surface Analysis, RSA) 3D-QSAR models to quantitatively predict the binding affinity of human adenosine A<sub>3</sub> receptor antagonists. Moreover, we have also reported a novel GPCR modeling approach, called Ligand-Based Homology Modeling (LBHM), as a tool to simulate the conformational changes of the receptor induced by ligand binding. In the present study, the application of both linear and nonlinear 3D-QSAR methods and LBHM computational techniques has been used to depict the hypothetical antagonist binding site of the human adenosine A<sub>2A</sub> receptor. In particular, a collection of 127 known human A<sub>2A</sub> antagonists has been utilized to derive two 3D-QSAR models (*autoMEPs*/PLS&RSA). In parallel, using a rhodopsin-driven homology modeling approach, we have built a model of the human adenosine A<sub>2A</sub> receptor. Finally, 3D-QSAR and LBHM strategies have been utilized to predict the binding affinity of five new human A<sub>2A</sub> pyrazolo-triazolo-pyrimidine antagonists finding a good agreement between the theoretical and the experimental predictions.

## INTRODUCTION

The integration of ligand- and structure-based strategies might sensitively increase the success of the drug discovery process.<sup>1</sup> In fact, ligand-based approaches are widely and successfully used to develop quantitative models able to correlate and predict the biological activities based on various molecular properties (molecular descriptors). On the other hand, referring to molecular docking simulations, the robustness of different scoring functions to estimate the ligand-target binding affinities is still very feeble, and this is particularly true when the 3D structure of a target molecule comes from homology modeling techniques or from low-resolution X-ray data as in the case of G protein-coupled receptors (GPCRs).<sup>1</sup> In particular, the rhodopsin-based homology modeling (RBHM) represents a very well consolidated approach to generate GPCR three-dimensional models.<sup>2,3</sup> Of course, the molecular docking can exhaustively explore the conformational space of a ligand inside its binding cavity, inferring on the possible ligand “bioactive” conformation. The bioactive conformation represents the

crucial starting point of all 3D-QSAR strategies such as Comparative Molecular Field Analysis (CoMFA)<sup>1,4</sup> or 3D-Pharmacophore search.<sup>1</sup> Therefore, the molecular docking poses might represent a natural “structural” input of a conventional 3D-QSAR when no other evidence concerning a “bioactive” pose is available.

As anticipated, 3D-QSAR methods require the knowledge of the conformational properties of the molecules in order to calculate their structural or property descriptors. Comparative Fields Analysis (CoMFA) is probably one of the most successfully used 3D-QSAR methods in medicinal chemistry in the last two decades.<sup>4</sup> Recently, we have reported that the *autocorrelation* Molecular Electrostatic Potential (*autoMEP*) vectors in combination with Partial Least-Square (PLS) analysis can represent an alternative 3D-QSAR tool to CoMFA.<sup>5–7</sup> Incidentally, both CoMFA and *autoMEP*/PLS methodologies can be classified as *linear* QSAR methods considering the mathematical relationship among molecular descriptors and chemical/biological response space. Very recently, we have also presented a nonlinear method based on a response surface analysis (RSA) application in tandem with the *autoMEP* descriptors (*autoMEP*/RSA) as an alternative *nonlinear* 3D-QSAR method.<sup>8,9</sup>

Moreover, recently we have also focused our attention on an alternative approach to computationally explore the multiconformational space of the antagonist-like state of GPCRs and, in particular, of the human adenosine A<sub>3</sub>

\* Corresponding author phone: +39 049 8275704; fax: +39 049 8275366; e-mail: stefano.moro@unipd.it.

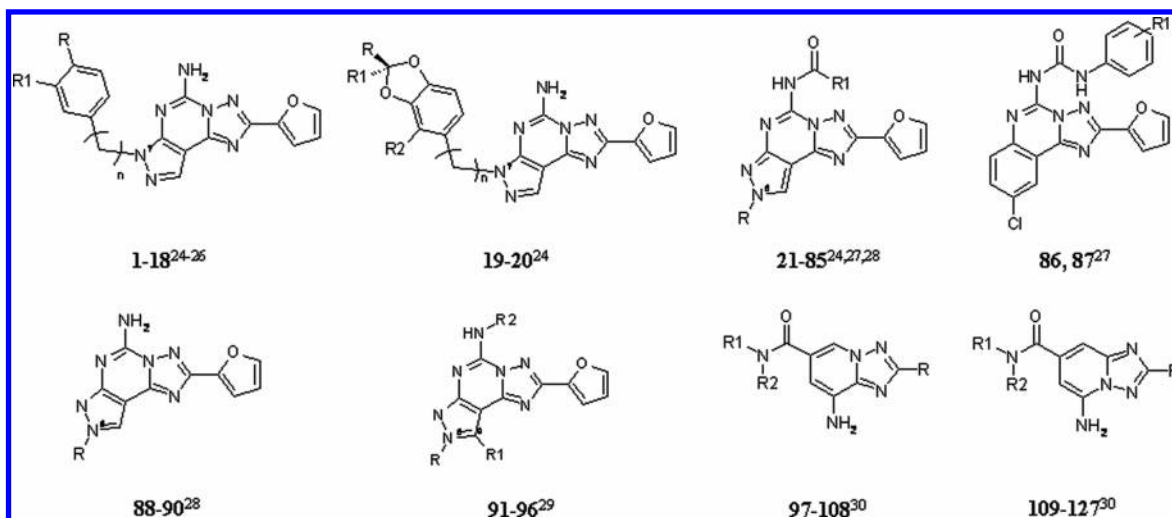
<sup>†</sup> Università di Padova.

<sup>‡</sup> Università di Trieste.

<sup>§</sup> Università degli Studi di Ferrara.

<sup>||</sup> Universität of Würzburg.

<sup>⊥</sup> Yamatake Corporation.



**Figure 1.** Chemical structures of known pyrazolo-triazolo-pyrimidine and triazolo-pyridine human A<sub>2A</sub> antagonists.

receptor.<sup>9–11</sup> In fact, the specificity (complementarity) of the ligand–receptor recognition process has been regarded for a long time as a critical feature of the receptor concept, even when the nature of the receptors was entirely unknown. Following this assumption, it is reasonable to expect that both pharmacological agonist and antagonist-like states can be described by several different conformational receptor states depending on the nature of both ligand and receptor. Indeed, considering different ligand–receptor complementarities, we might explore different conformations of the same pharmacological state. We have consequently developed a Ligand-Based Homology Modeling (LBHM) technique as a new approach to simulate the reorganization of the receptor induced by the ligand binding.<sup>10–13</sup>

In the present paper, we would like to present how the applicability of both linear and nonlinear 3D-QSAR methods (*auto*MEP/PLS&RSA) in combination with the LBHM technique can help to predict binding affinity data of a new set of human adenosine A<sub>2A</sub> receptor antagonists and clarify the possible receptor–ligand binding site.

Briefly, the adenosine A<sub>2A</sub> receptors are classified in the adenosine receptor (ARs) family of GPCRs, which includes A<sub>1</sub>, A<sub>2A</sub>, A<sub>2B</sub>, and A<sub>3</sub> different subtypes, abundantly expressed in diverse areas of the human body and potentially in the same cellular types.<sup>14</sup> Moreover, they are codified by distinct genes, and they have been cloned from various mammalian species, where they seem to differentiate for their pharmacological profile.<sup>14</sup> In particular, the human adenosine A<sub>2A</sub> receptor has been discovered to be crucial in some neurological disorders, which involve other neurotransmission systems too, above all the dopamine D<sub>2</sub> receptor, antagonistically associated with this adenosine receptor subtype.<sup>15</sup> It has been demonstrated that the activation of the human A<sub>2A</sub> receptor causes the inhibition of platelet aggregation, attenuates the inflammatory responses mediated by cytokines, and involves the regulation of the immune cells functions, while adenosine A<sub>2A</sub> receptor antagonists show a neuroprotective activity during ischemic processes.<sup>16</sup> The inhibition of the A<sub>2A</sub> receptor, blocking the effects of adenosine, has been suggested as a key strategy for the treatment of diverse pathologies.<sup>17</sup> In more detail, one of the main potential therapeutic applications of A<sub>2A</sub> receptor antagonists is the promotion of cellular survival and the reduction of neuronal

damage in Parkinson's or Huntington's diseases.<sup>17–20</sup> In the past few years, several different potent and selective human adenosine A<sub>2A</sub> receptor antagonists have been discovered.<sup>21</sup> In particular, pyrazolo-triazolo-pyrimidine and triazolo-pyridine derivatives have been described as promising human A<sub>2A</sub> receptor antagonists,<sup>21–23</sup> and their chemical structures are summarized in Figure 1.

In the present study, a collection of 127 known human A<sub>2A</sub> antagonists has been utilized to derive two 3D-QSAR models (*auto*MEP/PLS&RSA). In parallel, using a rhodopsin-driven homology modeling approach, we have built a model of the human adenosine A<sub>2A</sub> receptor. Finally, 3D-QSAR and LBHM strategies have been utilized to predict the binding affinity of five new human A<sub>2A</sub> pyrazolo-triazolo-pyrimidine antagonists, following the flow chart shown in Figure 2.

## MATERIALS AND METHODS

**Computational Methodologies.** All modeling studies were carried out on a linux cluster running under openMosix architecture.<sup>31</sup>

The autocorrelation MEP descriptors have been carried out using the Adriana (version 2.0) suite.<sup>32</sup> Partial Least-Square (PLS) analysis has been performed using “The Unscrambler” statistical software.<sup>33</sup> Response Surface Analysis (RSA) has been performed using DataFOREST<sup>34</sup> and DataNESIA<sup>35</sup> softwares.

Homology modeling, Ligand-based Homology Modeling (LBHM), potential energy calculations and docking studies have been performed using the Molecular Operating Environment (MOE, version 2006.08) suite.<sup>36</sup>

All docked structures have been fully optimized without geometry constraints using RHF/AM1 semiempirical calculations. The vibrational frequency analysis has been used to characterize the minima stationary points (zero imaginary frequencies). The software package MOPAC (version 7),<sup>37</sup> implemented into the MOE suite, has been utilized for all quantum mechanical calculations.

**Molecular Structure Building.** 3D models of all human A<sub>2A</sub> receptor antagonists were obtained by using the 3D structure generator Corina. Corina is an integral part of the Adriana suite.<sup>32</sup> Conformers generation and the best con-

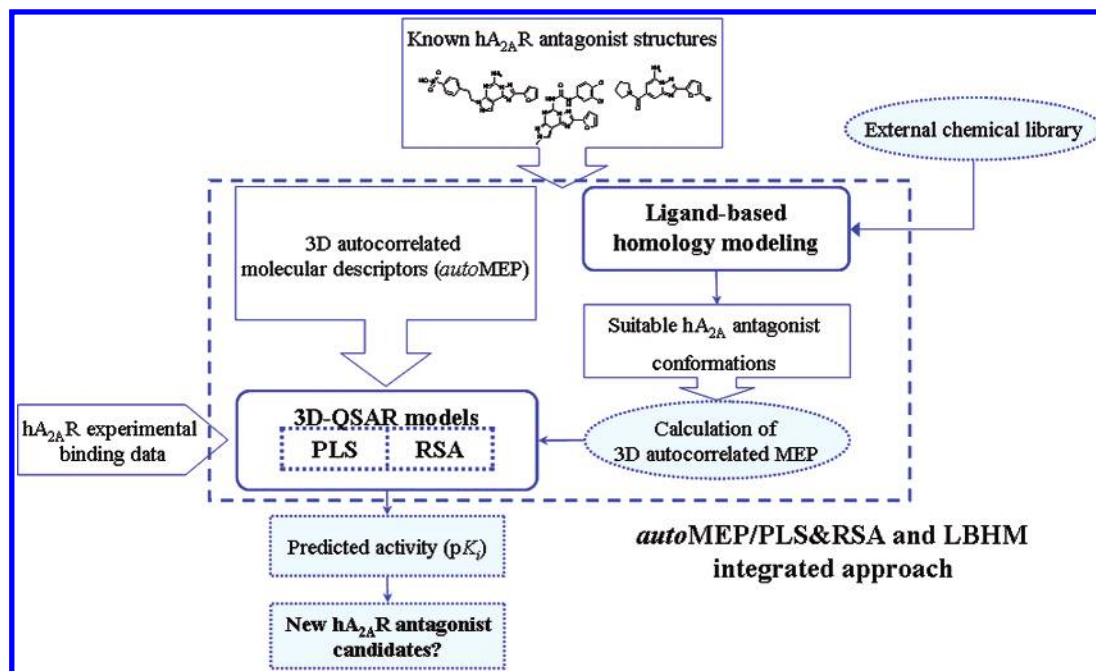


Figure 2. Flowchart of the integrated *autoMEP/PLS&RSA* and *LBHM* approach using for scouting new human  $A_{2A}$  receptor antagonist.

former selection have been carried out using standard parameters of Corina. Conformer selection is one of the most crucial steps in every 3D-QSAR approaches. In this specific key study, due to the very limited information about the possible binding mode of all known  $A_{2A}$  receptor antagonists (1–137), we have decided to select the energetically most stable conformers produced by Corina conformational analysis. On the contrary, for the new synthesized derivatives 138–142, the conformations used for all QSAR studies were selected from our molecular docking studies (the most stable docking poses), as described in detail in the “molecular docking of the human adenosine  $A_{2A}$  receptor antagonists” paragraph reported below. Protonation states are selected in agreement with the corresponding  $pK_a$  at the physiological pH value (7.4 unit).

**Training Set.** As summarized in Figure 1, a collection of 127 pyrazolo-triazolo-pyrimidine and triazolo-pyridine analogues (1–127) has been selected as training set in both linear- and nonlinear QSAR models.<sup>24–30</sup> The complete list of both structures and pharmacological binding data are collected in the Supporting Information.

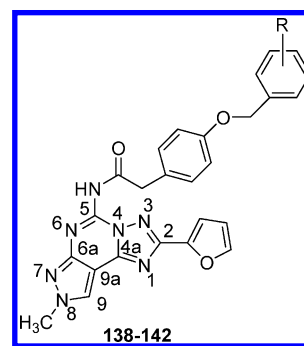
**Test Sets.** An *internal* test set of 10 training set analogues (128–137) has been selected for the validation process of both PLS and RSA models.

Finally, five new pyrazolo-triazolo-pyrimidine analogues (138–142) have been analyzed as an additional (*external*) validation set. Structures and pharmacological profiles of all new synthesized antagonists are reported in Table 1.

**Molecular Electrostatic Potential (MEP) Calculation.** In the present work, MEPs derive from a classical point charge model: the electrostatic potential for each molecule is obtained by moving a unit positive point charge across the molecular surface, and it is calculated at various points  $j$  on this surface by the following equation

$$V_j = \sum_i^{\text{atoms}} \frac{q_i}{r_{ji}}$$

Table 1. Biological Profile of the New Synthesized Pyrazolo-Triazolo-Pyrimidines Derivatives 138–142



no.	R	$hA_1$ ( $K_i$ nM) <sup>a</sup>	$hA_{2A}$ ( $K_i$ nM) <sup>b</sup>	$hA_{2B}$ ( $IC_{50}$ nM) <sup>c</sup>	$hA_3$ ( $K_i$ nM) <sup>d</sup>
138	H	2640 (2200–3180)	233 (205–265)	12900 (11100–15100)	29.4 (14.8–58.1)
139	2-CH <sub>3</sub>	2940 (2680–3230)	333 (217–511)	>30000 (4.93–9.35)	6.80 (4.93–9.35)
140	2,6-Cl	1680 (1480–1900)	281 (221–357)	17800 (12600–25200)	35.3 (17.8–70)
141	3-Cl	1980 (1890–2070)	278 (235–329)	10400 (8900–12.200)	9.93 (6.35–15.5)
142	4-CH <sub>3</sub>	6760 (4180–10900)	751 (594–950)	>30000 (22.5–26.5)	24.4 (22.5–26.5)

<sup>a</sup> Displacement of specific [<sup>3</sup>H]-CCPA binding at human  $A_1$  receptors expressed in CHO cells ( $n = 3–6$ ). <sup>b</sup> Displacement of specific [<sup>3</sup>H]-NECA binding at human  $A_{2A}$  receptors expressed in CHO cells. <sup>c</sup>  $IC_{50}$  values of the inhibition of NECA-stimulated adenylyl cyclase ( $A_{2B}$ ) activity in CHO cells expressing  $hA_{2B}$  receptors. <sup>d</sup> Displacement of specific [<sup>3</sup>H]-NECA binding at human  $A_3$  receptors expressed in CHO cells. Data are expressed as geometric means, with 95% confidence limit.

where  $q_i$  represents the partial charge of each atom  $i$ , and  $r_{ji}$  is the distance between points  $j$  and atom  $i$ . Starting from the 3D model of a molecule and its partial atomic charges, the electrostatic potential or another appropriate property is calculated for points on the molecular surface. Partial atomic



charges were calculated by the PEOE (Partial Equalization of Orbital Electronegativity) method and its extension to conjugated systems implemented by the Petra (Parameter Estimation for the Treatment of Reactivity Applications) module of the Adriana suite.<sup>32,38–39</sup> Connolly's solvent accessible surface with a solvent radius of 2.0 Å has been used to project the corresponding MEP. Once the autocorrelation function has been applied, the autocorrelation vector is obtained. Connolly's solvent accessible surfaces and the corresponding MEPs have been calculated by the Surface module of the Adriana suite.<sup>32</sup>

**Autocorrelation MEP (autoMEP) Vectors.** The idea of using autocorrelation for the transformation of the constitution of a molecule into a fixed length representation was introduced by Moreau and Broto.<sup>40,41</sup> A certain property,  $p_k$ , of an atom  $i$  is correlated with the same property of atom  $j$ , and these products are summed over all atom pairs having a certain topological distance  $d$ . Each component of the autocorrelation vector is calculated as follows

$$A(d) = \sum_{ij} p_i p_j$$

where  $A$  is the autocorrelation coefficient referring to atom pairs  $i, j$ ,  $p_i$  is the atomic property, and  $d$  is the  $i, j$  topological distance.

Ligands and proteins interact through molecular surfaces, and, therefore, clearly, the representations of molecular surfaces have to be sought in the endeavor to understand the biological activity. Again, we are under the restriction of having to represent molecular surfaces of different size; and again, autocorrelation was employed to achieve this goal.<sup>42–44</sup> First, a set of randomly distributed points on the molecular surface has to be generated. Then, all distances between the surface points are calculated and sorted into preset intervals

$$A(d_{\text{lower}}, d_{\text{upper}}) = 1/L \sum p_i p_j (d_{\text{lower}} < d_{ij} < d_{\text{upper}})$$

where the  $i, j$  distance  $d$  belongs to the  $d_{\text{lower}}, d_{\text{upper}}$  interval, and  $L$  is number of distances in the same interval. The application of this concept made it possible to compare different molecular properties, as this 3D descriptor represents a compressed expression of the distribution of the property  $p$  on the molecular surface. The parameters for the calculation of the autocorrelation coefficient are the following:  $d_{\text{lower}} = 1$  Å;  $d_{\text{upper}} = 13$  Å;  $L = 12$ ; point density = 10 points/Å<sup>2</sup>; vdW radius reduction factor = 1.000. All parameters have been changed in a various way to see if it was possible to improve the model capability, but nonsignificance results were derived. Considering the distances from 1 to 13 Å, with a step width of 1 Å, twelve autocorrelation coefficients are calculated. This transformation produces a unique fingerprint of each molecule under consideration. The autocorrelation vectors have been calculated by the Surface module of the Adriana suite.<sup>32</sup>

**Partial Least-Square (PLS) Analysis.** Conventional PLS analysis has been carried out as previously reported for the human A<sub>3</sub> receptor antagonists.<sup>5–7</sup>

**Response Surface Analysis (RSA).** Response surface analysis (RSA) is a collection of mathematical and statistical techniques useful for analyzing the effects of several

independent variables.<sup>45</sup> In most RSA problems, the relationship between the response and the independent variables is unknown. Thus, the first step in RSA is to approximate the function ( $f$ ). Usually, this process employs a low-order polynomial in some region of the independent variables. If the response is well-modeled by a linear function of the independent variables, then the approximating function is a first-order model. If there is curvature in the system or in the region of the optimum, then a polynomial of higher degree must be used to approximate the response, which is analyzed to locate the optimum, i.e., the set of independent variables such that the partial derivatives of the model response with respect to the individual independent variables is equal to zero. The eventual objective of RSA is to determine the optimum operating conditions for the system or to determine a region which satisfies the operating specifications. Almost all RSA problems utilize one or both of these approximating polynomials.

In this work, our RSA is based on a multivariate *thin plate spline* algorithm<sup>46</sup> derived by the Green's theorem and implemented into the DataNESIA suite<sup>35</sup>

$$y = \sum_{i=1}^n \alpha_i g(d_i) + \sum_{j=1}^p c_j x_j$$

where  $\alpha_i$  and  $c_j$  are the weight coefficients,  $p$  is the number of the independent variables  $x$ ,  $n$  is the number of data points, and  $d_i$  is the Green's function applied to the Euclidean distances between data  $i$  and any coordinate in the  $x$ -axis. According to this algorithm, the response surface function is the result of an elastic beam displacement in the  $x_n$  space, where the elastic beam has to bend to reach the data points in the  $y$  space.<sup>46</sup> Input values are therefore regarded as points of force actions, while output values are regarded as displaced values.

In the RSA technique, the selection of the most informative independent variables (in our specific case, *autoMEP* descriptors) is strongly recommended to reduce the dimensionality of the final model and improve model predictivity. Using the DataFOREST suite,<sup>34</sup> a linear stepwise regression and a nonlinear cluster analysis have been applied to select the most statistically relevant independent *autoMEP* descriptors to use in our RSA technique.

**autoMEP/PLS&RSA Application.** Both PLS and RSA techniques have been carried out in parallel, and the performances of both models were compared following the flow chart shown in Figure 3. We have also verified if a *consensus* strategy might improve robustness and predictivity of the final model.

**Homology Model of the Human Adenosine A<sub>2A</sub> Receptor.** Based on the assumption that GPCRs share similar TM boundaries and overall topology, a homology model of the human adenosine A<sub>2A</sub> receptor has been constructed. First, the amino acid sequences of TM helices of the A<sub>2A</sub> receptor were aligned with those of the bovine rhodopsin, guided by the highly conserved amino acid residues, including the DRY motif (D3.49, R3.50, and Y3.51) and three proline residues (P4.60, P6.50, and P7.50) in the TM segments of GPCRs. The same boundaries were applied for the TM helices of the A<sub>2A</sub> receptor as they were identified from the X-ray crystal structure for the corresponding sequences of the

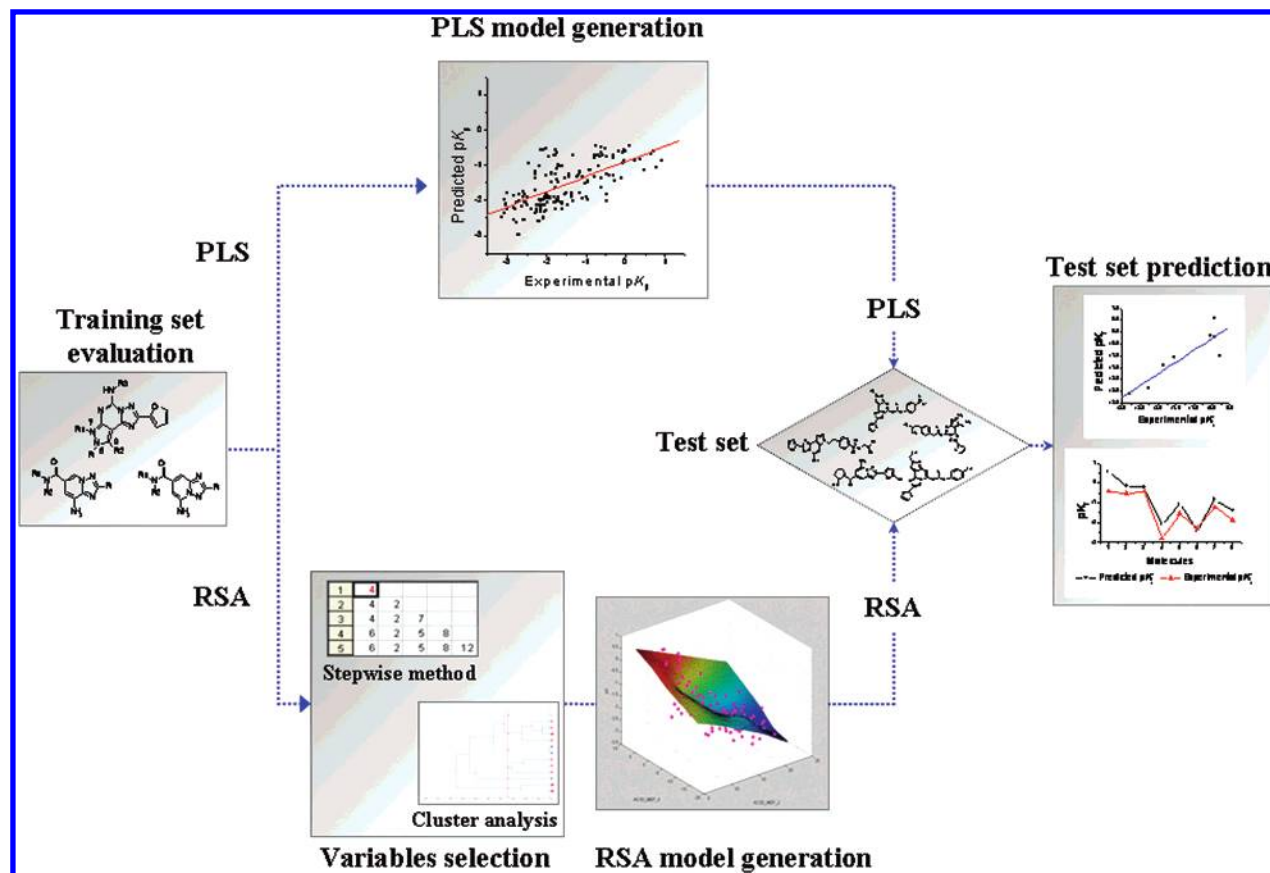


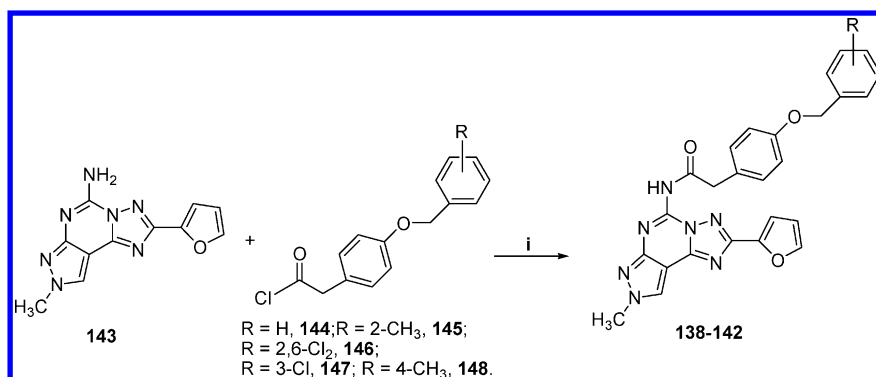
Figure 3. Partial Least-Square (PLS) and Response Surface Analysis (RSA) approaches.

bovine rhodopsin, the  $C_R$  coordinates of which were used to construct the seven TM helices for the human  $A_{2A}$  receptor.<sup>47</sup> The loop domains of the human  $A_{2A}$  receptor were constructed by the loop search method implemented in MOE. In particular, loops are modeled first in random order. For each loop, a contact energy function analyzes the list of candidates collected in the segment searching stage, taking into account all atoms already modeled and any atoms specified by the user as belonging to the model environment. These energies are then used to make a Boltzmann-weighted choice from the candidates, the coordinates of which are then copied to the model. Any missing side chain atoms are modeled using the same procedure. Side chains belonging to residues whose backbone coordinates were copied from a template are modeled first, followed by side chains of modeled loops. Outgaps and their side chains are modeled last. Special caution has to be given to the second extracellular (EL2) loop, which has been described in the bovine rhodopsin as folding back over transmembrane helices and, therefore, limiting the size of the active site.<sup>47</sup> Hence, amino acids of this loop could be involved in direct interactions with the ligands. A driving force to this peculiar fold of the EL2 loop might be the presence of a disulfide bridge between cysteines in TM3 (Cys77, 3.25) and EL2 (Cys166). Since this covalent link is conserved in all receptors modeled in the current study, the EL2 loop was modeled using a rhodopsin-like constrained geometry around the EL2-TM3 disulfide bridge. After the heavy atoms were modeled, all hydrogen atoms were added, and the protein coordinates were then minimized with MOE using the AMBER94 force field.<sup>48</sup> The minimizations were carried out by the 1000 steps of steepest descent followed by conjugate gradient minimization

until the rms gradient of the potential energy was less than  $0.1 \text{ kcal mol}^{-1} \text{ \AA}^{-1}$ . Protein stereochemistry evaluation was performed by several tools (Ramachandran and Chi plots measure phi/psi and chi1/chi2 angles, clash contacts reports) implemented in the MOE suite.<sup>36</sup>

**Ligand-Based Homology Modeling (LBHM).** We have recently revisited the rhodopsin-based model of the human  $A_3$  receptor in its resting state (antagonist-like state), taking into account a novel strategy to simulate the possible receptor reorganization induced by the antagonist-binding. We called this new strategy ligand-based homology modeling.<sup>11–13</sup> This computational methodology has been also utilized in the optimization step of all antagonist- $A_{2A}$  receptor complexes. Briefly, ligand-based homology modeling technique is an evolution of a conventional homology modeling strategy that combined the Boltzmann-weighted randomized modeling procedure adapted from Levitt with a specialized algorithm for the proper handling of insertions and deletions of any selected extra-atoms during the energy tests and minimization stages of the modeling procedure.<sup>36,49</sup> Ligand-based homology modeling option is very useful when one wishes to build a homology model in the presence of a ligand docked to the primary template, or other proteins known to be complexed with the sequence to be modeled.<sup>36</sup> In this specific case both model building and refinement take into account the presence of the ligand in terms of specific steric and chemical features. In order to generate an initial ensemble of ligand poses, a conventional docking procedure (see next section for details) with reduced van der Waals radii (equal to 75%) and an increased Coulomb-vdW cutoff (cutoff on 10 Å; cutoff on 12 Å) was performed. For each pose, a homology model is then generated to accommodate the ligand by reorienting

Scheme 1



nearby side chains. These residues and the ligand are then locally minimized. Finally, each ligand is redocked into its corresponding low-energy protein structure, and the resulting complexes are ranked according to MOE-Score.<sup>36</sup>

Different quantitative measurements of molecular volume of the receptor binding cavities were carried out using the MOE suite.<sup>36</sup> Prediction of the antagonist-receptor complex stability (in terms of the corresponding  $pK_i$  value) and the quantitative analysis for nonbonded intermolecular interactions (H-bonds, transition metal, water bridges, hydrophobic) were calculated and visualized using several tools implemented in the MOE suite.<sup>36</sup>

**Molecular Docking of the Human Adenosine A<sub>2A</sub> Receptor Antagonists.** All antagonist structures were docked into the hypothetical TM binding site by using the MOE-DOCK tool, part of the MOE suite. Searching is conducted within a user-specified 3D docking box (the standard protocol selects all atoms inside 12 Å from the center of mass of the binding cavity), using the Tabu Search protocol (standard parameters are 1000 steps/run, 10 attempts/step, and 10 Tabu list length)<sup>50</sup> and the MMFF94 force field.<sup>51</sup> MOE-Dock performs a user-specified number of independent docking runs (50 in our specific case) and writes the resulting conformations and their energies in a molecular database file. The resulting docked complexes were subjected to MMFF94 energy minimization until the rms of conjugate gradient was  $<0.1 \text{ kcal mol}^{-1} \text{ Å}^{-1}$ . Charges for the ligands were imported from the MOPAC output files. To better refine all antagonist-receptor complexes, a rotamer exploration of all side chains involved in the antagonist-binding was carried out. The rotamer exploration methodology was implemented in the MOE suite.<sup>36</sup>

**Chemistry.** The new synthesized A<sub>2A</sub> antagonists **138–142** were prepared starting from the 8-amino pyrazolo-triazolo-pyrimidine **143**<sup>52,53</sup> by a coupling reaction with the appropriate acyl chloride (**144–148**) in freshly distilled tetrahydrofuran in the presence of triethylamine, as shown in Scheme 1. The acyl chlorides were obtained by treatment with thionyl chloride in the presence of a catalytic amount of DMF of the corresponding carboxylic acids.<sup>54</sup>

**General.** Reactions were routinely monitored by thin-layer chromatography (TLC) on silica gel (precoated F<sub>254</sub> Merck plates). Infrared spectra (IR) were measured on a Jasco FT-IT instrument. <sup>1</sup>H NMR were determined in CDCl<sub>3</sub> or DMSO-d<sub>6</sub> solutions with a Varian Gemini 200 spectrometer, peaks positions are given in parts per million ( $\delta$ ) downfield from tetramethylsilane as internal standard, and *J* values are given in Hz. Light petroleum ether refers to the fractions

boiling at 40–60 °C. Melting points were determined on a Buchi-Tottoli instrument and are uncorrected. Flash chromatography was performed using Merck 60–200 mesh silica gel. Elemental analyses were performed at the microanalytical laboratory of Dipartimento di Chimica, University of Trieste, and were within  $\pm 0.4\%$  of the theoretical values for C, H, and N.

**General Procedures for the Preparation of Acyl-amino-8-methyl-2-(2-furyl)pyrazolo[4,3-e]1,2,4-triazolo[1,5-c]pyrimidine (**138–142**).** The amino compound (**143**, 0.25 g, 1 mmol) was dissolved in freshly distilled THF (10 mL), and appropriate acyl chloride **144–148** (1.3 mmol) and triethylamine (0.32 mL, 1.3 mmol) were added. The mixture was refluxed under argon for 18 h. Then the solvent was removed under reduced pressure, and the residue was dissolved in EtOAc (30 mL) and washed twice with water (15 mL). The organic phase was dried on Na<sub>2</sub>SO<sub>4</sub> and concentrated under reduced pressure. The residue was purified by flash chromatography (EtOAc-light petroleum 4:6) to afford the desired compounds (**138–142**).

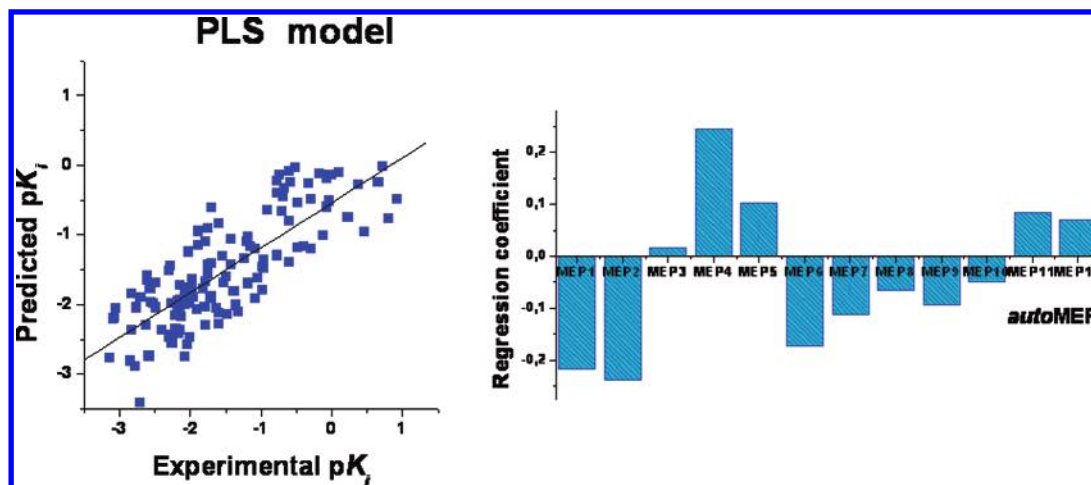
**5-[[4-(Benzyloxy)]phenylacetyl]amino-8-methyl-2-(2-furyl)pyrazolo[4,3-e]1,2,4-triazolo[1,5-c]pyrimidine (**138**).** yield 83%, yellow solid; mp 148 °C (EtOAc-light petroleum); IR (KBr): 3235–2990, 1675, 1610, 1570, 1520 cm<sup>-1</sup>; <sup>1</sup>H NMR (DMSO-d<sub>6</sub>)  $\delta$ : 3.90 (s, 2H); 4.11 (s, 3H); 5.06 (s, 2H); 4.99 (s, 2H); 6.79 (dd, 1H, *J* = 2, *J* = 4); 6.92 (d, 2H, *J* = 9); 7.07–7.35 (m, 8H); 7.37 (d, 2H, *J* = 9); 7.94 (d, 1H, *J* = 2); 8.77 (s, 1H); 10.82 (bs, 1H). Anal. (C<sub>26</sub>H<sub>21</sub>N<sub>7</sub>O<sub>3</sub>) C, H, N.

**5-[[4(2-Methylbenzyloxy)]phenylacetyl]amino-8-methyl-2-(2-furyl)pyrazolo[4,3-e]1,2,4-triazolo[1,5-c]pyrimidine (**139**).** yield 70%, yellow solid; mp 135 °C (EtOAc-light petroleum); IR (KBr): 3230–2980, 1670, 1620, 1550, 1510 cm<sup>-1</sup>; <sup>1</sup>H NMR (DMSO-d<sub>6</sub>)  $\delta$ : 2.25 (s, 3H); 3.99 (s, 2H); 4.15 (s, 3H); 5.55 (s, 2H); 6.73 (dd, 1H, *J* = 2, *J* = 4); 6.85–7.45 (m, 9H); 7.61 (d, 1H, *J* = 2); 8.06 (s, 1H); 9.85 (bs, 1H). Anal. (C<sub>27</sub>H<sub>23</sub>N<sub>7</sub>O<sub>3</sub>) C, H, N.

**5-[[4(2,6-Dichlorobenzyloxy)]phenylacetyl]amino-8-methyl-2-(2-furyl)pyrazolo[4,3-e]1,2,4-triazolo[1,5-c]pyrimidine (**140**).** yield 80%, pale yellow solid; mp 151 °C (EtOAc-light petroleum); IR (KBr): 3230–2975, 1668, 1625, 1570, 1505 cm<sup>-1</sup>; <sup>1</sup>H NMR (DMSO-d<sub>6</sub>)  $\delta$ : 3.99 (s, 2H); 4.20 (s, 3H); 4.47 (s, 2H); 6.60 (dd, 1H, *J* = 2, *J* = 4); 6.97 (d, 2H, *J* = 9); 7.03–7.32 (m, 6H); 7.88 (d, 1H, *J* = 2); 8.07 (s, 1H); 9.25 (bs, 1H). Anal. (C<sub>26</sub>H<sub>19</sub>N<sub>7</sub>O<sub>3</sub>Cl<sub>2</sub>) C, H, N.

**5-[[4(3-Chlorobenzyloxy)]phenylacetyl]amino-8-methyl-2-(2-furyl)pyrazolo[4,3-e]1,2,4-triazolo[1,5-c]pyrimidine (**141**).** yield 77%, yellow solid; mp 183 °C (EtOAc-light petroleum);





**Figure 4.** AutoMEP/PLS model: (on the left) experimental  $pK_i$  data plotted vs predicted  $pK_i$  (after cross-validation) values of the training set; (on the right) variables influence plot (VIP) reporting the weight of each descriptor in the PLS model.

**Table 2.** Summary of Statistical Parameters of the autoMEP/PLS Model

	PLS model
number of molecules	127
latent variables	3
$r$	0.80
$r_{cv}^a$	0.78
$r_{bs}^b$	0.79
slope	0.62
offset	-0.57
$q^c$	0.85
RMR <sup>d</sup>	0.043

<sup>a</sup> Cross-validated  $r$  after leave-one-out procedure:  $r_{cv} = [SXY / (SXX)^{1/2}(SYY)^{1/2}]$ ,  $SXY = \sum(X - X_{mean})(Y - Y_{mean})$ ,  $SXX = \sum(X - X_{mean})^2$ , and  $SYY = \sum(Y - Y_{mean})^2$  with  $X = Y_{experimental}$  and  $Y = Y_{predicted}$ . <sup>b</sup> Cross-validated  $r$  after bootstrapping process. <sup>c</sup>  $r$  of the internal test set. <sup>d</sup> Root-mean-square of residuals.

IR (KBr): 3230–2970, 1665, 1625, 1580, 1515  $\text{cm}^{-1}$ ;  $^1\text{H}$  NMR (DMSO- $d_6$ )  $\delta$ : 4.18 (s, 3H); 4.43 (s, 2H); 5.00 (s, 2H); 6.58 (dd, 1H,  $J = 2, J = 4$ ); 6.96 (d, 2H,  $J = 9$ ); 7.03–7.38 (m, 6H); 7.40 (s, 1H); 7.73 (d, 1H,  $J = 2$ ); 8.19 (s, 1H); 9.08 (bs, 1H). Anal. ( $\text{C}_{26}\text{H}_{20}\text{N}_7\text{O}_3\text{Cl}$ ) C, H, N.

5-[[4(4-Methylbenzyloxy)]phenylacetyl]amino-8-methyl-2-(2-furyl)pyrazolo[4,3-*e*]1,2,4-triazolo[1,5-*c*]pyrimidine (**142**). yield 77%, brown solid; mp 128  $^\circ\text{C}$  (EtOAc-light petroleum); IR (KBr): 3240–2985, 1677, 1618, 1570, 1525  $\text{cm}^{-1}$ ;  $^1\text{H}$  NMR (DMSO- $d_6$ )  $\delta$ : 2.23 (s, 3H); 3.98 (s, 2H); 4.18 (s, 3H); 4.65 (s, 2H); 6.83 (dd, 1H,  $J = 2, J = 4$ ); 6.98 (d, 2H,  $J = 9$ ); 7.05 (d, 2H,  $J = 9$ ); 7.25 (d, 1H,  $J = 4$ ); 7.27 (d, 2H,  $J = 9$ ); 7.29 (d, 2H,  $J = 9$ ); 7.85 (d, 1H,  $J = 2$ ); 8.23 (s, 1H); 9.25 (bs, 1H). Anal. ( $\text{C}_{27}\text{H}_{23}\text{N}_7\text{O}_3$ ) C, H, N.

**Biology.** Binding at the Human Adenosine  $A_1$ ,  $A_{2A}$ , and  $A_3$  Receptors. All pharmacological methods followed the procedures as described earlier.<sup>55</sup> In brief, membranes for radioligand binding were prepared from CHO cells stably transfected with the human adenosine receptor subtypes in a two-step procedure. In a first low-speed step (1000  $\times$  g) cell fragments and nuclei were removed. The crude membrane fraction was sedimented from the supernatant at 100 000  $\times$  g. The membrane pellet was resuspended in the buffer used for the respective binding experiments, frozen in liquid nitrogen, and stored at  $-80\text{ }^\circ\text{C}$ . For the measurement of the adenylyl cyclase activity only one high-speed centrifugation of the homogenate was used. The resulting crude

membrane pellet was resuspended in 50 mM Tris/HCl, pH 7.4 and immediately used for the cyclase assay.

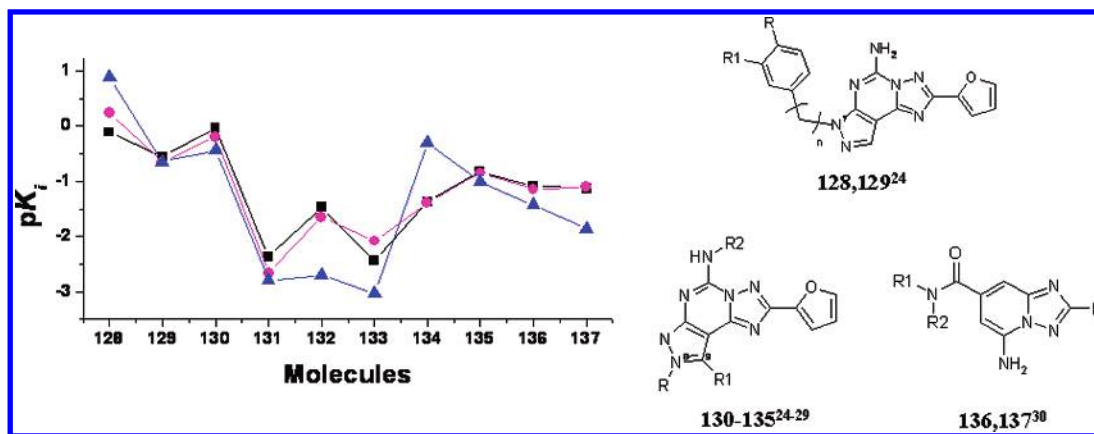
For radioligand binding at adenosine  $A_1$  receptors 1 nM [ $^3\text{H}$ ]CCPA was used, whereas 30 and 10 nM [ $^3\text{H}$ ]NECA were used for  $A_{2A}$  and  $A_3$  receptors, respectively. Nonspecific binding of [ $^3\text{H}$ ]CCPA was determined in the presence of 1 mM theophylline; in the case of [ $^3\text{H}$ ]NECA 100  $\mu\text{M}$  R-PIA was used.<sup>56</sup>

**Adenylyl Cyclase Activity.** Due to the lack of a suitable radioligand the potency of antagonists was determined in adenylyl cyclase experiments. The procedure was carried out as described previously with minor modifications.<sup>55,57</sup> Membranes were incubated with about 150 000 cpm of [ $\alpha$ - $^{32}\text{P}$ ]ATP for 20 min in the incubation mixture as described without EGTA and NaCl.<sup>55,57</sup> For agonists the  $\text{EC}_{50}$ -values for the stimulation of adenylyl cyclase were calculated with the Hill equation. Hill coefficients in all experiments were near unity.  $\text{IC}_{50}$  values for concentration-dependent inhibition of NECA-stimulated adenylyl cyclase caused by antagonists was calculated accordingly. The dissociation constants ( $K_i$ ) for the antagonists were then calculated with the Cheng and Prusoff equation.<sup>58</sup> A summary of binding data of the five compounds is shown in Table 1.

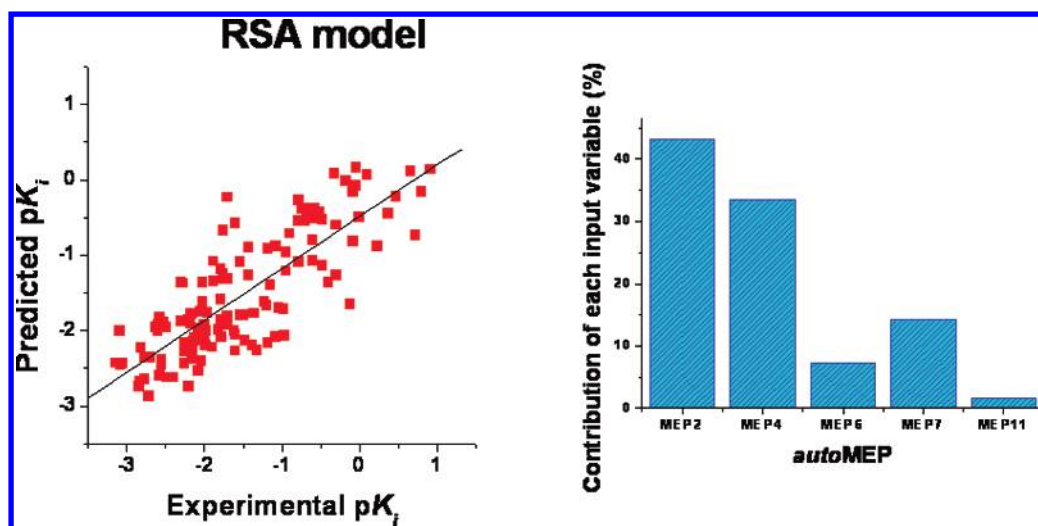
## RESULTS AND DISCUSSION

Topological and electrostatic complementarities are considered two key concepts in the molecular recognition processes. Gasteiger and collaborators investigated the MEP on a molecular surface as a particularly useful method for rationalizing the interactions between molecules and molecular recognition processes.<sup>42–44</sup> Moreover, the introduction of the autocorrelation vector allows for overcoming the MEP information inconvenience to be reliant on the spatial rotation and translation of the molecule. We have already demonstrated that the autoMEP vectors can be used as interesting molecular descriptors in different 3D-QSAR applications.<sup>5–9</sup>

In this work, using the above-described autoMEP vectors, we have verified the possibility of combining two different linear and nonlinear 3D-QSAR strategies, such as PLS and RSA, with a receptor-based approach to prioritize the synthesis of new human  $A_{2A}$  antagonists. In particular, we have merged together the information of the quantitative binding affinity predictions, coming from the two QSAR



**Figure 5.** Comparison of *autoMEP/PLS* (■) and *autoMEP/RSA* predicted  $pK_i$  (●) with the experimental  $pK_i$  values (▲) of the *internal test set*. Relative scaffolds are displayed on the right.



**Figure 6.** *AutoMEP/RSA* model: (on the left) experimental  $pK_i$  data plotted vs predicted  $pK_i$  values (after cross-validation) of the training set; (on the right) variable influence plot (VIP) reporting the % contribution of each descriptor in the RSA model.

techniques, with the qualitative information derived from by the analysis of the receptor–ligand complementarities, obtained by our ligand-based homology modeling strategy.

**PLS and RSA QSAR Models.** Both 3D-QSAR models have been derived by using 96 pyrazolo-triazolo-pyrimidine and 31 triazolo-pyridine derivatives as a training set of known A<sub>2A</sub> receptor antagonists. Moreover, both models have been subjected to a validation process by using a test set of 10 molecules (defined as the *internal test set*, **128–137**) structurally related to those included into the training set.

As already described, twelve *autoMEP* vectors have been used as independent variables in both PLS and RSA analyses; moreover, a preliminary variable selection step has been introduced before running the RSA technique (see the Experimental Section for more details).

Concerning PLS analysis, the resulting model has shown acceptable statistical quality in both calibration and internal validation steps as demonstrated by the  $r$  and  $r_{cv}$  values of 0.80 and 0.78, respectively, using only three latent variables (Figure 4 and Table 2).

The robustness of the PLS model is also supported by the good value of the correlation coefficient calculated on the test set ( $q = 0.85$ ) (Figure 5 and Table 2).

In parallel, we have delivered a nonlinear RSA model using the same training and test data sets. The stepwise regression analysis together with the cluster analysis on the

**Table 3.** Summary of Statistical Parameters of the *autoMEP/RSA* Model

	RSA model
number of molecules	127
X variables	5
$r$	0.98
$r_{cv}^a$	0.82
slope	0.68
offset	−0.49
$q^b$	0.87
RMR <sup>c</sup>	0.043

<sup>a</sup> Cross-validated  $r$  after leave-one-out procedure:  $r_{cv} = [SXY / (SXX)^{1/2}(SYY)^{1/2}]$ ,  $SXY = \sum(X - X_{mean})(Y - Y_{mean})$ ,  $SXX = \sum(X - X_{mean})^2$ , and  $SYY = \sum(Y - Y_{mean})^2$  with  $X = Y_{experimental}$  and  $Y = Y_{predicted}$ . <sup>b</sup>  $r$  of the internal test set. <sup>c</sup> Root-mean-square of residuals.

original 12 molecular descriptors led us to select five of them as final combination independent variables for the RSA model: *autoMEP* 2, 4, 6, 7, and 11. We can notice that these descriptors are recognized as very important even in PLS analysis. (Figure 4) The statistical parameters and the final RSA model are collected in Figure 6 and Table 3.

We can observe a very high correlation coefficient value ( $r = 0.98$ ) for the calibration step confirming the good choice of the independent variables selection. The correlation coefficient of the test set is also appreciable ( $r_{cv} = 0.82$ ). Finally, a very good correlation coefficient calculated on the



**Table 4.** Predicted and Experimental  $pK_i$  for the *Internal* Test Set

no.	exptl $pK_i$	pred $pK_i$	pred $pK_i$	$\Delta pK_i^a$	$\Delta pK_i^a$
		autoMEP/ PLS	autoMEP/ RSA	autoMEP/ PLS	autoMEP/ RSA
128	0.89	-0.11	0.25	-1.00	-0.64
129	-0.64	-0.55	-0.65	0.09	-0.01
130	-0.43	-0.04	-0.20	0.39	0.23
131	-2.79	-2.36	-2.66	0.43	0.13
132	-2.70	-1.47	-1.65	1.23	1.05
133	-3.02	-2.44	-2.08	0.58	0.94
134	-0.29	-1.37	-1.39	-1.08	-1.10
135	-1.00	-0.82	-0.85	0.18	0.15
136	-1.43	-1.08	-1.14	0.35	0.29
137	-1.86	-1.13	-1.11	0.73	0.75

<sup>a</sup> Predicted  $pK_i$  - experimental  $pK_i$ .

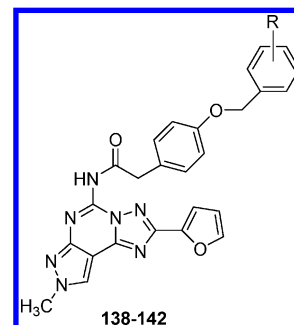
test set ( $q = 0.87$ ) is an additional evidence about the good predictivity of the *autoMEP*/RSA model.

Even if both methods are statistically acceptable, the *autoMEP*/RSA model presents higher predictivity than PLS, as reported in Table 4. However, both methodologies are able to coherently discriminate between “more active” and “less active” analogues. This is very interesting because ensemble, or *consensus*, approaches to classification and regression have attracted a great deal of interest in recent years.<sup>59</sup> In fact, consensus strategies have been shown to outperform single predictor usability on a wide range of scientific applications.<sup>59</sup> In this study, we used both *autoMEP*/PLS and RSA models as an ensemble of binding affinity predictors to prioritize the synthesis of new human  $A_{2A}$  antagonists.

Following these encouraging results, we have tested the real predictive capability of our PLS&RSA models on an additional test set (*external* test set), which consisted of five new pyrazolo-triazolo-pyrimidine analogues (**138–142**). Even if we are aware about the limited number of compounds selected in this preliminary *additional* test set, we would like to utilize it as a preliminary proof of concept of our *tandem* PLS&RSA approach. As anticipated in the Introduction, the main goal to simultaneously perform different 3D-QSAR approaches, such as PLS and RSA, is the possibility to create a more even balance between false positive and false negative performance rates than use of a single method can achieve.

In our laboratories, we are still developing new potent and selective human  $A_{2A}$  antagonists decorating the pyrazolo-triazolo-pyrimidine scaffold using different strategies.<sup>60</sup> In this contest, we analyzed a new class of N<sup>5</sup>-substituted derivatives in which a different serie of benzyloxy-phenyl-acetyl substituents is present. Once molecular descriptors (*autoMEP* vectors) have been computed for this new set of ligands, we have passed the data through both PLS and RSA models for their binding affinity predictions. As shown in Table 5, both methods have predicted all five derivatives active in the low nM range ( $K_i$  values in between 50 and 150 nM), with a better performance of the *autoMEP*/RSA model with respect to PLS, as found in our preliminary validation step. Interesting, even if both methods overestimate all binding affinities, new synthesized pyrazolo-triazolo-pyrimidine analogues are active in the nM range ( $K_i$  values in between 230 and 750 nM), as theoretically predicted (Figure 7).

**Human  $A_{2A}$  Ligand-Based Homology Modeling.** To deciphering the observed structure–activity relationship and

**Table 5.** Predicted and Experimental  $pK_i$  for the new Synthesized Pyrazole-Triazolo-Pyrimidines Derivatives **138–142**

no.	R	exptl $pK_i$	pred $pK_i$	pred $pK_i$	$\Delta pK_i^a$	$\Delta pK_i^a$
			autoMEP/ PLS	autoMEP/ RSA	autoMEP/ PLS	autoMEP/ RSA
138	H	-2.37	-1.96	-2.14	0.41	0.22
139	3-CH <sub>3</sub>	-1.40	-1.86	-1.95	-0.46	-0.55
140	2,6-Cl	-2.45	-1.83	-1.94	0.62	0.51
141	3-Cl	-2.44	-1.67	-1.98	0.78	0.46
142	4-CH <sub>3</sub>	-1.41	-1.82	-1.97	-0.41	-0.56

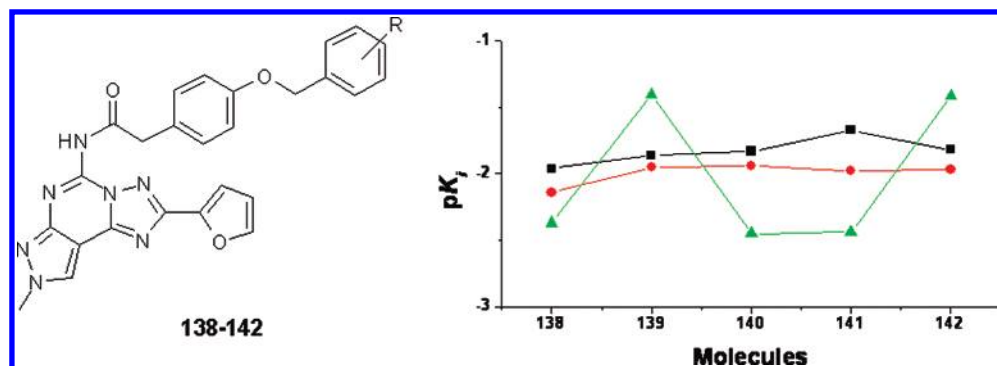
<sup>a</sup> Predicted  $pK_i$  - experimental  $pK_i$ .

correlate the ligand affinities to a suitable receptor-antagonist binding motif, we decided to build up a three-dimensional model of the human  $A_{2A}$  receptor.

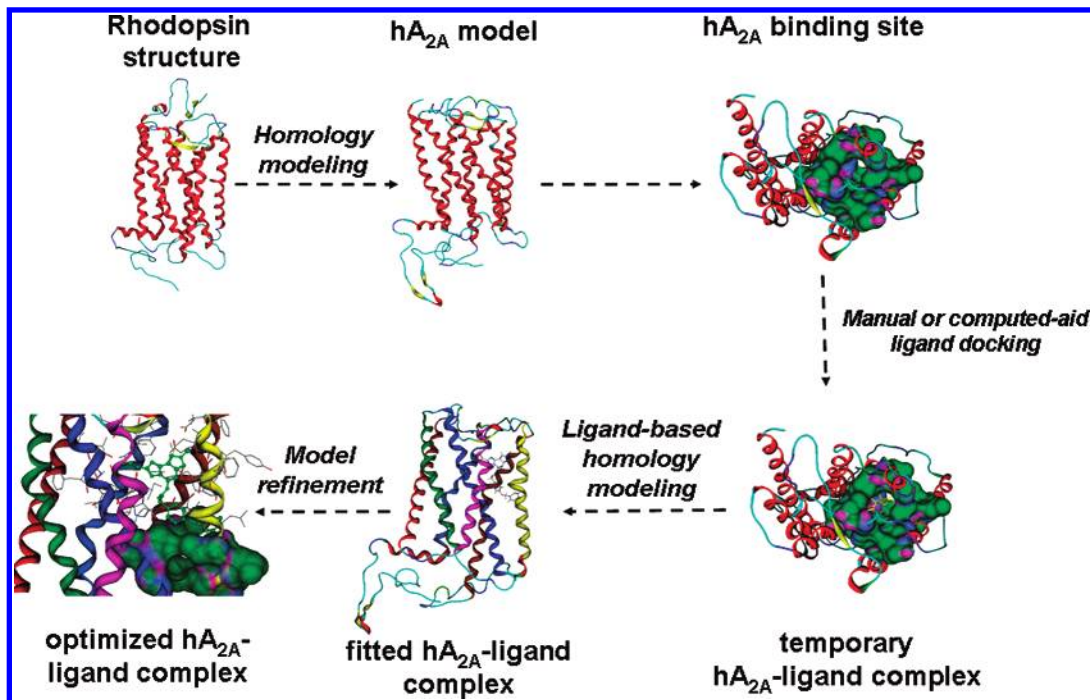
The human  $A_{2A}$  receptor shares 49% amino acid sequence identity with the human  $A_1$  receptor, 58% with the human  $A_{2B}$  subtype, and only 41% with the human  $A_3$  receptor. As all other members of Family A-GPCRs, the general topology of the human  $A_{2A}$  receptor is preserved consisting of a typical 3–4 type helix–helix contact associated with optimal interactions between nearly parallel aligned helices. Following our previously reported modeling studies, we have constructed a new refined model of the human  $A_{2A}$  receptor by using a rhodopsin-based homology modeling (RBHM) approach.<sup>3,10,61–66</sup> Moreover, our recently described ligand-based homology modeling (LBHM) approach has been used to simulate the conformational changes induced by the ligand binding, and a schematic representation of the ligand-based homology protocol is shown in Figure 8 (methodological details are summarized in the Materials and Methods section).<sup>10–13</sup>

As reported in Figure 9, depending on the topological properties of the different ligands, we found two different conformational models of the human  $A_{2A}$  receptor reverse agonist-like state in which both shape and chemical complementarities have been specifically optimized around each ligand. Pyrazole-triazolo-pyrimidines derivative **63** has been used as a reference derivative to optimize the human  $A_{2A}$  receptor cavity obtained by using the conventional rhodopsin-based homology modeling.

In this specific case, with the varying of the ligand structure, the molecular volume of the transmembrane (TM) binding cavity changes from the 660 Å<sup>3</sup> of the standard RBHM-driven model to the 1330 Å<sup>3</sup> of the largest LBHM-driven model, without altering the conventional rhodopsin-like receptor topology. The modifications of both shape and volume of the human  $A_{2A}$  TM binding cavity are the most important receptor modeling perturbations obtained by the application of the LBHM technique. The binding cavity reorganization induced by the ligand binding might be due



**Figure 7.** Experimental  $pK_i$  activity data (▲) of the *external* test set compared to  $pK_i$  values predicted by *autoMEP/PLS* (■) and *autoMEP/RSA* models (●). Molecular scaffold is reported on the left.



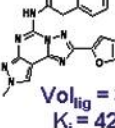


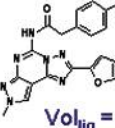

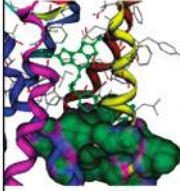
**Figure 8.** Flowchart of the ligand-based homology modeling (LBHM) technique considering an evolution of a conventional rhodopsin-based homology modeling (RBHM) approach.

to the conformational change in several amino acid side chains, such as the following: Val94 (3.32), Leu95 (3.33), Thr98 (3.36), Gln99 (3.37), Ile102 (3.40), Gln167 (EL2), Phe168 (EL2), Phe192 (5.43), Val196 (5.47), Leu190 (5.51), Phe242 (6.44), Trp246 (6.48), Leu247 (6.49), Met270 (7.35), Ile274 (7.39). In addition, the larger LBHM-model 2 other amino acids such as Ile92 (3.30), Leu190 (5.41), and Met193 (5.44) seem to be involved in the induce fit mediate by bulkier antagonists. However, the molecular docking studies carried out for all pyrazole-triazolo-pyrimidines antagonists, using the appropriate conformational states of the receptor as listed in Figure 9, have shown a similar binding motif indicating that a common receptor-driven pharmacophore model can be depicted. This finding is coherent with our previously reported studies for this class of antagonists versus the human A<sub>3</sub> receptor.<sup>3,10,61–66</sup> Interestingly, none of the new pyrazole-triazolo-pyrimidine antagonists have found an energetically stable docking pose in the conventional RBHM-driven A<sub>2A</sub> model (TM volume cavity ca. 660 Å<sup>3</sup>). This is mainly due to the unfavorable topological complementarity among these antagonists and the corresponding RBHM-driven TM binding cavity. In particular, highly destabilizing

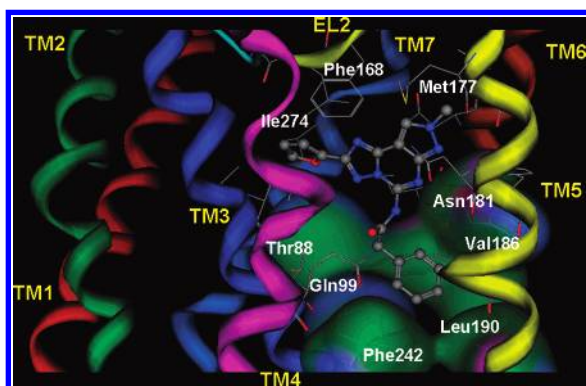
van der Waals interactions (steric conflicts) seem to be the reason of lacking topological complementarities. These steric conflicts are drastically reduced or completely eliminated after the application of the LBHM approach.

As shown in Figure 10, the ligand recognition occurs in the upper region of the TM bundle, and the pyrazole-triazolo-pyrimidines moiety is surrounded by TMs 3, 5, 6, 7 with the substituent in the N<sup>5</sup>-position oriented toward the intracellular environment. The furan ring is positioned between TM3 and TM7, whereas the N<sup>8</sup>-substituents are surrounded by TM3 and TM5. Interestingly, these pharmacophore feature models are nicely coherent with our recently proposed human A<sub>3</sub>-based pharmacophore model.

Analyzing in detail our model, all pyrazolo-triazolo-pyrimidine derivatives present the carbamoyl moiety in the 5-position surrounded by two polar amino acids: Gln89 (3.37) and His250 (6.52). This region seems to be very critical for the recognition of the antagonist structures, and both amino acids are mutated in the human A<sub>3</sub> receptor. In fact, a major structural difference between the hypothetical binding sites is that the A<sub>3</sub> receptor does not contain the histidine residue in TM6 common to all A<sub>1</sub> (His251 in hA<sub>1</sub>)

Reference derivative	Docked derivatives	Rhodopsin-based homology model $Vol_{cav} \approx 660 \text{ \AA}^3$	LBHM: model 1 (using compound <b>63</b> as reference structure) $Vol_{cav} \approx 995 \text{ \AA}^3$	LBHM: model 2 (using compound <b>138</b> as reference structure) $Vol_{cav} \approx 1330 \text{ \AA}^3$
<b>Compound 63</b>  $Vol_{lig} = 337 \text{ \AA}^3$ $K_i = 423 \text{ nM}$		NO REASONABLE DOCKING POSES		
<b>Compound 138</b>  $Vol_{lig} = 444 \text{ \AA}^3$ $K_i = 223 \text{ nM}$	<b>compounds 139–142</b> 	NO REASONABLE DOCKING POSES	NO REASONABLE DOCKING POSES	

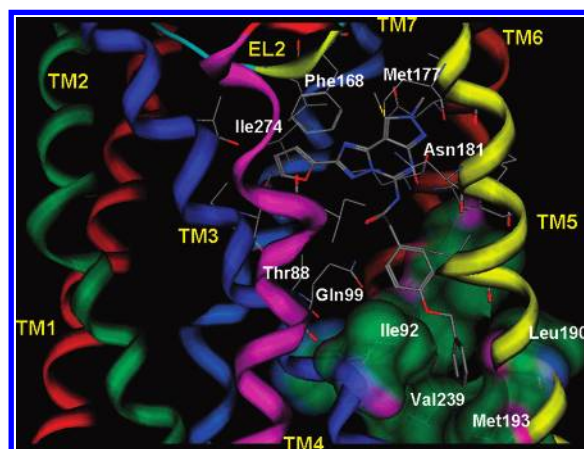
**Figure 9.** Ligand-Based Homology Modeling (LBHM) data collection. Each “reference derivative” (compounds **63** and **138**) was used as a ligand-template during the homology modeling process. Consequently, four different conformational states (*models 1–2*) were selected as putative ambassadors of the conformational changes induced by different ligand binding. Depending on their different structure topologies, all other antagonists (*docked derivatives*) were docked into the most complementary receptor models.



**Figure 10.** Hypothetical binding motif of the reference compound **63** docked into the LBHM-model of the human  $A_{2A}$  adenosine receptor. The most energetically favorable docked conformation is viewed from the membrane side facing. Side chains of some amino acids important for the ligand recognition are highlighted. Hydrogen atoms are not displayed. The receptor region around the 4-position of the aryl ring, characterized by three nonpolar amino acids Val186 (5.47), Leu190 (5.51), and Phe242 (6.44), has been represented by its Connolly's molecular surface.

and  $A_2$  (His250 in  $hA_{2A}$  and His251 in  $hA_{2B}$ ) receptors. This histidine has been shown to participate in both agonist and antagonist binding to the  $A_{2A}$  receptor. In the  $A_3$  receptor this histidine in TM6 is replaced by a serine residue (Ser247 in  $hA_3$ ). On the other side, the highly conserved glutamine residue in TM3 (Gln92 in  $hA_1$ , Gln89 in  $hA_{2A}$  and Gln90 in  $hA_{2B}$ ) is replaced by a histidine in the human  $A_3$  receptor (His95).

The stabilizing interactions among the carbamoyl moiety and these polar amino acids orient the carbamoyl phenyl ring in the middle of the TM bundle. In particular, the side chain of Gln89 (3.37) is within hydrogen-bonding distance of NH of the carbamoyl group of the ligand at 2.6 Å. Moreover, the N–H of His250 (6.52) and the oxygen atom of the carbamoyl group are separated by 3.8 Å and appropriately oriented to form an H-bonding interaction. According to the recently published mutagenesis results in the human  $A_3$ ,



**Figure 11.** Hypothetical binding motif of the new synthesized compound **138** docked into the LBHM-model2 of the human  $A_{2A}$  adenosine receptor. The most energetically favorable docked conformation is viewed from the membrane side facing. Side chains of some amino acids important for the ligand recognition are highlighted. Hydrogen atoms are not displayed. The receptor region by three nonpolar amino acids Ile92 (3.30), Leu190 (5.41), and Met193 (5.44) has been represented by its Connolly's molecular surface.

His95 (3.37) is crucial for the ligand recognition, whereas Ser247 (6.52) slightly affects the binding of both agonists and antagonists.<sup>67</sup>

Similar to the  $A_3$  receptor, the receptor region around the aryl ring of the carbamoyl moiety is mostly hydrophobic and characterized by four nonpolar amino acids: Ile92 (3.40), Val186 (5.47), Phe242 (6.44), and Leu247 (6.49). The evaluation of the ligand binding pocket of this specific region of the  $A_{2A}$  receptor reveals that an empty space is present between TM5 and TM6, and consequently the 4-position of the aryl ring could be decorated with other substituents.

Starting from this antagonist binding hypothesis, we decided to validate our  $A_{2A}$  receptor model exploring the possibility of accommodating a bulky substituent at the 4-position of the aryl ring. All five pyrazolo-triazolo-



pyrimidine analogues (**138–142**) can nicely fit inside the remodeled binding cavity (Figure 9, LBHM-model 2). As shown in Figure 11, the hypothetical binding motif is very similar to that already described to the reference compound **63**.

In particular, the bulky substituent at the 4-position of the aryl ring seems to be located deeply in the TM region surrounded by the following amino acids: Ile92 (3.30), Leu190 (5.41), and Met193 (5.44). As anticipated, these amino acids seem to be involved in the induce fit mediated by these bulkier antagonists. As already reported,<sup>12,13,66</sup> this hydrophobic region is also conserved into the human adenosine A<sub>3</sub> receptor binding cleft, and it could explain the high A<sub>3</sub> binding affinity reported in Table 1. Consequently, the molecular docking results based on our LBHM receptor model confirm that all derivatives **138–142** can be efficiently recognized by the A<sub>2A</sub> receptor binding cavity.

### CONCLUSIONS

Considering that GPCR ligands represent not only one of the major classes of current drugs but also the major continuing source of novel potent pharmaceutical agents and that 3D structures of GPCRs as determined by experimental techniques are still unavailable, ligand-based drug discovery methods remain the major computational molecular modeling approaches to the analysis of growing data sets of tested GPCR ligands.

In the present paper the application of two complementary QSAR methodologies in tandem with a receptor-based ligand design strategy has been used to evaluate the recognition of a new series of human A<sub>2A</sub> antagonists. Two statistically meaningful models have been generated from a common training set, and their predictivity has been verified by using both internal and external test sets. A rhodopsin-based model of the human A<sub>2A</sub> receptor has been built up to qualitatively describe the hypothetical binding mode of these classes of known human A<sub>2A</sub> receptor antagonists. Moreover, the combination of this receptor-based approach with the QSAR studies is a very interesting example of integration between ligand- and receptor based drug design techniques. In our lab, we are continuously analyzing a new set of ligands with the aim to improve the robustness and the predictivity of our QSAR models using, when possible, high throughput docking as a conformational selector for the calculation of our 3D-driven chemical descriptors. Moreover, using our computational protocol, an intense virtual screening campaign is also being carried out to discover new potent and selective human A<sub>2A</sub> receptor antagonists.

### ACKNOWLEDGMENT

The molecular modeling work coordinated by S.M. was carried out with financial support from the University of Padova, Italy, and the Italian Ministry for University and Research (MIUR), Rome, Italy. We thank the Molecular Network GmbH (Erlangen, Germany) for the assistance in using the Adriana modeling suite. S.M. is also very grateful to the Chemical Computing Group for the scientific and technical partnership.

**Supporting Information Available:** Training set (Table 1) and test set (Table 2). This material is available free of charge via the Internet at <http://pubs.acs.org>.

### REFERENCES AND NOTES

- (1) Moro, S.; Bacilieri, M.; Deflorian, F. Combining Ligand-Based and Structure-Based Drug Design in the Virtual Screening Arena. *Expert Opin. Drug Discovery* **2007**, *2*, 37–49.
- (2) Fanelli, F.; De Benedetti, P. G. Computational Modeling Approaches to Structure-Function Analysis of G Protein-Coupled Receptors. *Chem. Rev.* **2005**, *105*, 3297–3351.
- (3) Moro, S.; Spalluto, G.; Jacobson, K. A. Techniques: Recent Developments in Computer-Aided Engineering of GPCR Ligands Using the Human A<sub>3</sub> Adenosine Receptor as an Example. *Trends Pharmacol. Sci.* **2005**, *26*, 44–51.
- (4) Cramer, R. D. I.; Patterson, D. E.; Bunce, J. D. Comparative Molecular Field Analysis (CoMFA). 1. Effect of Shape on Binding of Steroids to Carrier Proteins. *J. Am. Chem. Soc.* **1988**, *110*, 5969–5967.
- (5) Moro, S.; Bacilieri, M.; Ferrari, C.; Spalluto, G. Autocorrelation of Molecular Electrostatic Potential Surface Properties Combined with Partial Least Squares Analysis as Alternative Attractive Tool to Generate Ligand-Based 3D-QSARs. *Curr. Drug Discovery. Technol.* **2005**, *2*, 13–21.
- (6) Moro, S.; Bacilieri, M.; Cacciari, B.; Spalluto, G. Autocorrelation of Molecular Electrostatic Potential Surface Properties Combined with Partial Least Squares Analysis as New Strategy for the Prediction of the Activity of Human A<sub>3</sub> Adenosine Receptor Antagonists. *J. Med. Chem.* **2005**, *48*, 5698–5704.
- (7) Moro, S.; Bacilieri, M.; Cacciari, B.; Bolcato, C.; Cusan, C.; Pastorin, G.; Klotz, K. N.; Spalluto, G. The Application of a 3D-QSAR (autoMEP/PLS) Approach as an Efficient Pharmacodynamic-Driven Filtering Method for Small-Sized Virtual Library: Application to a Lead Optimization of a Human A<sub>3</sub> Adenosine Receptor Antagonist. *Bioorg. Med. Chem.* **2006**, *14*, 4923–4932.
- (8) Bacilieri, M.; Kaseda, C.; Spalluto, G.; Moro, S. Response Surface Analysis as Alternative 3D-QSAR Tool: Human A<sub>3</sub> Adenosine Receptor Antagonists as a Key Study. *Lett. Drug Des. Discovery* **2007**, *4*, 122–127.
- (9) Bacilieri, M.; Varano, F.; Deflorian, F.; Marini, M.; Catarzi, D.; Colotta, V.; Filacchioni, G.; Galli, A.; Costagli, C.; Kaseda, C.; Moro, S. Tandem 3D-QSARs Approach as Valuable Tool to Predict Binding Affinity Data: Design of New Gly/NMDA Receptor Antagonists as a Key Study. *J. Chem. Inf. Model.* **2007**, in press.
- (10) Moro, S.; Bacilieri, M.; Deflorian, F.; Spalluto, G. G Protein-Coupled Receptors as Challenging Druggable Targets: Insights from in Silico Studies. *New J. Chem.* **2006**, *30*, 301–308.
- (11) Moro, S.; Deflorian, F.; Bacilieri, M.; Spalluto, G. Ligand-Based Homology Modeling as Attractive Tool to Inspect GPCR Structural Plasticity. *Curr. Pharm. Des.* **2006**, *12*, 2175–2185.
- (12) Colotta, V.; Catarzi, D.; Varano, F.; Capelli, F.; Lenzi, O.; Filacchioni, G.; Martini, C.; Trincavelli, L.; Ciampi, O.; Pugliese, A. M.; Pedata, F.; Schiesaro, A.; Morizzo, E.; Moro, S. New 2-Arylpyrazolo[3,4-c]-quinoline Derivatives as Potent and Selective Human A<sub>3</sub> Adenosine Receptor Antagonists. Synthesis, Pharmacological Evaluation and Ligand-Receptor Modeling Studies. *J. Med. Chem.* **2007**, *50*, 4061–4074.
- (13) Bolcato, C.; Cusan, C.; Pastorin, G.; Spalluto, G.; Cacciari, B.; Klotz, K. N.; Morizzo, E.; Moro, S. Pyrazolo-triazolo-pyrimidines as Adenosine Receptor Antagonists: Effect of the N-5 Bond Type on the Affinity and Selectivity at the Four Adenosine Receptor Subtypes. *Purinergic Signalling*, **2007**, in press, DOI: 10.1007/s11302–007-9058-y.
- (14) Fredholm, B. B.; Arslan, G.; Halldner, L.; Kull, B.; Schulte, G.; Wasserman, W. Structure and Function of Adenosine Receptors and their Genes. *Naunyn-Schmiedeberg's Arch. Pharmacol.* **2000**, *362*, 364–374.
- (15) Ferre, S.; Von, Euler, G.; Johansson, B.; Fredholm, B. B.; Fuxe, K. Stimulation of High-Affinity Adenosine A<sub>2</sub> Receptors Decreases the Affinity of Dopamine D<sub>2</sub> Receptors in Rat Striatal Membranes. *Proc. Natl. Acad. Sci. U.S.A.* **1991**, *88*, 7238–7241.
- (16) Ribeiro, J. A.; Sebastiao, A. M.; De Mendonca, A. Adenosine Receptors in the Nervous System: Pathophysiological Implications. *Prog. Neurobiol.* **2002**, *68*, 377–392.
- (17) Jacobson, K. A.; Gao, Z. G. Adenosine Receptors as Therapeutic Targets. *Nat. Rev. Drug Discovery* **2006**, *5*, 247–264.
- (18) Xu, K.; Bastia, E.; Schwarzschild, M. Therapeutic Potential of Adenosine A<sub>2A</sub> Receptor Antagonists in Parkinson's Disease. *Pharmacol. Ther.* **2005**, *105*, 267–310.
- (19) Pinna, A.; Volpini, R.; Cristalli, G.; Morelli, M. New Adenosine A<sub>2A</sub> Receptor Antagonists: Actions on Parkinson's Disease Models. *Eur. J. Pharmacol.* **2005**, *512*, 157–164.
- (20) Johnston, T. H.; Brotchie, J. M. Drugs in Development for Parkinson's Disease: an Update. *Curr. Opin. Invest. Drugs* **2006**, *7*, 25–32.
- (21) Cristalli, G.; Cacciari, B.; Dal, Ben, D.; Lambertucci, C.; Moro, S.; Spalluto, G.; Volpini, R. Highlights on the Development of A<sub>2A</sub>

- Adenosine Receptor Agonists and Antagonists. *Chem. Med. Chem.* **2007**, *2*, 260–281.
- (22) Baraldi, P. G.; Cacciari, B.; Borea, P. A.; Varani, K.; Pastorin, G.; Da Ros, T.; Tabrizi, M. A.; Fruttarolo, F.; Spalluto, G. Pyrazolo-triazolo-pyrimidine Derivatives as Adenosine Receptor Antagonists: a Possible Template for Adenosine Receptor Subtypes? *Curr. Pharm. Des.* **2002**, *8*, 2299–2332.
  - (23) Moro, S.; Gao, Z. G.; Jacobson, K. A.; Spalluto, G. Progress in the Pursuit of Therapeutic Adenosine Receptor Antagonists. *Med. Res. Rev.* **2006**, *26*, 131–159.
  - (24) Baraldi, P. G.; Tabrizi, M. A.; Bovero, A.; Avitabile, B.; Preti, D.; Fruttarolo, F.; Romagnoli, R.; Varani, K.; Borea, P. A. Recent Developments in the Field of A<sub>2A</sub> and A<sub>3</sub> Adenosine Receptor Antagonists. *Eur. J. Med. Chem.* **2003**, *38*, 367–382.
  - (25) Baraldi, P. G.; Cacciari, B.; Romagnoli, R.; Spalluto, G.; Monopoli, A.; Ongini, E.; Varani, K.; Borea, P. A. 7-Substituted 5-amino-2-(2-furyl)pyrazolo[4,3-e]-1,2,4-triazolo[1,5-c]pyrimidines as A<sub>2A</sub> Adenosine Receptor Antagonists: a Study on the Importance of Modifications at the Side Chain on the Activity and Solubility. *J. Med. Chem.* **2002**, *45*, 115–126.
  - (26) Baraldi, P. G.; Cacciari, B.; Spalluto, G.; Bergonzoni, M.; Dionisotti, S.; Ongini, E.; Varani, K.; Borea, P. A. Design, Synthesis, and Biological Evaluation of a Second Generation of Pyrazolo[4,3-e]-1,2,4-triazolo[1,5-c]pyrimidines as Potent and Selective A<sub>2A</sub> Adenosine Receptor Antagonists. *J. Med. Chem.* **1998**, *41*, 2126–2133.
  - (27) Baraldi, P. G.; Cacciari, B.; Moro, S.; Spalluto, G.; Pastorin, G.; Da Ros, T.; Klotz, K. N.; Varani, K.; Gessi, S.; Borea, P. A. Synthesis, Biological Activity, and Molecular Modeling Investigation of New Pyrazolo[4,3-e]-1,2,4-triazolo[1,5-c]pyrimidine Derivatives as Human A<sub>3</sub> Adenosine Receptor Antagonists. *J. Med. Chem.* **2002**, *45*, 770–780.
  - (28) Baraldi, P. G.; Cacciari, B.; Romagnoli, R.; Spalluto, G.; Varani, K.; Gessi, S.; Merighi, S.; Borea, P. A. Pyrazolo[4,3-e]-1,2,4-triazolo[1,5-c]pyrimidine Derivatives: a New Pharmacological Tool for the Characterization of the Human A<sub>3</sub> Adenosine Receptor. *Drug Dev. Res.* **2001**, *52*, 406–415.
  - (29) Baraldi, P. G.; Fruttarolo, F.; Tabrizi, M. A.; Preti, D.; Romagnoli, R.; El-Kashef, H.; Moorman, A.; Varani, K.; Gessi, S.; Merighi, S.; Borea, P. A. Design, Synthesis, and Biological Evaluation of C<sup>9</sup>- and C<sup>2</sup>-substituted Pyrazolo[4,3-e]-1,2,4-triazolo[1,5-c]pyrimidines as New A<sub>2A</sub> and A<sub>3</sub> Adenosine Receptors Antagonists. *J. Med. Chem.* **2003**, *46*, 1229–1241.
  - (30) Guba, W.; Nettekoven, M.; Pullmann, B.; Riemer, C.; Schmitt, S. Comparison of Inhibitory Activity of Isomeric Triazolopyridine Derivatives towards Adenosine Receptor Subtypes or Do Similar Structures Reveal Similar Bioactivities? *Bioorg. Med. Chem. Lett.* **2004**, *14*, 3307–3312.
  - (31) *OpenMosix*, version 2.4.26; Moshe Bar, Tel Aviv University: Israel, 2004.
  - (32) *Adriana*, version 2.0; Molecular Networks GmbH: Erlangen, Germany, 2003.
  - (33) *The Unscrambler*, version 9.2; CAMO Process AS: Oslo, Norway, 2003.
  - (34) *DataFOREST*, version 9; Yamatake Corporation: Fujisawa-shi Kanagawa, Japan, 2007.
  - (35) *DataNESIA*, version 3.2; Yamatake Corporation: Fujisawa-shi Kanagawa, Japan, 2007.
  - (36) *Molecular Operating Environment*, version 2006.08; Chemical Computing Group: Montreal, Canada, 2006.
  - (37) *MOPAC*, version 7; J. J. P. Stewart, Fujitsu Limited: Tokyo, Japan, 1993.
  - (38) Gasteiger, J.; Marsili, M. Iterative Partial Equalization of Orbital Electronegativity - a Rapid Access to Atomic Charges. *Tetrahedron* **1980**, *36*, 3219–3228.
  - (39) Gasteiger, J.; Saller, H. Calculation of the Charge Distribution in Conjugated Systems by a Quantification of the Resonance Concept. *Angew. Chem., Int. Ed. Engl.* **1985**, *24*, 687–689.
  - (40) Moreau, G.; Broto, P. The Autocorrelation of a Topological Structure: a New Molecular Descriptor. *Nouv. J. Chim.* **1980**, *4*, 359–360.
  - (41) Moreau, G.; Broto, P. Autocorrelation of Molecular Structures, Application to SAR Studies. *Nouv. J. Chim.* **1980**, *4*, 757–764.
  - (42) Gasteiger, J.; Li, X.; Rudolph, C.; Sadovski, J.; Zupan, J. Representation of Molecular Electrostatic Potential by Topological Feature Maps. *J. Am. Chem. Soc.* **1994**, *116*, 4608–4620.
  - (43) Wagener, M.; Sadovski, J.; Gasteiger, J. Autocorrelation of Molecular Surface Properties for Modeling Corticosteroid Binding Globulin and Cytosolic Ah Receptor Activity by Neural Networks. *J. Am. Chem. Soc.* **1995**, *117*, 7769–7778.
  - (44) Bauknecht, H.; Zell, A.; Bayer, H.; Levi, P.; Wagener, M.; Sadovski, J.; Gasteiger, J. Locating Biologically Active Compounds in Medium-Sized Heterogeneous Datasets by Topological Autocorrelation Vectors: Dopamine and Benzodiazepine Agonists. *J. Chem. Inf. Comput. Sci.* **1996**, *36*, 1205–1213.
  - (45) Myers, R.; Montgomery, D. C. *Response methodology surface*; John Wiley, Ed.; Wiley-Interscience: New York, U.S.A., 1995.
  - (46) Kaseda, C. *Response Surface Methodology using a spline algorithm*; G.d.a.c.S., Ed.; Nashboro Press: Fujisawa-shi Kanagawa, Japan, 2004.
  - (47) Palczewski, K.; Kumasaka, T.; Hori, T.; Behnke, C. A.; Motoshima, H.; Fox, B. A.; Le, Trong, I.; Teller, D. C.; Okada, T.; Stenkamp, R. E.; Yamamoto, M.; Miyano, M. Crystal Structure of Rhodopsin: A G Protein-Coupled Receptor. *Science* **2000**, *289*, 739–745.
  - (48) Cornell, W. D. C. P.; Bayly, C. I.; Gould, I. R.; Merz, K. M.; Ferguson, D. M.; Spellmeyer, D. C.; Fox, T.; Caldwell, J. W.; Kollman, P. A. A Second Generation Force Field for the Simulation of Proteins, Nucleic Acids and Organic Molecules. *J. Am. Chem. Soc.* **1995**, *117*, 5179–5196.
  - (49) Levitt, M. Accurate Modeling of Protein Conformation by Automatic Segment Matching. *J. Mol. Biol.* **1992**, *226*, 507–533.
  - (50) Baxter, C. A.; Murray, C. W.; Clark, D. E.; Westhead, D. R.; Eldridge, M. D. Flexible Docking Using Tabù Search and an Empirical Estimate of Binding Affinity. *Proteins: Struct., Funct. Genet.* **1998**, *33*, 367–382.
  - (51) Halgren, T. Merck Molecular Force Field. I. Basis, Form, Scope, Parameterization, and Performance of MMFF94. *J. Comput. Chem.* **1996**, *17*, 490–519.
  - (52) Baraldi, P. G.; Cacciari, B.; Romagnoli, R.; Spalluto, G.; Moro, S.; Klotz, K. N.; Leung, E.; Varani, K.; Gessi, S.; Merighi, S.; Borea, P. A. Pyrazolo[4,3-e]-1,2,4-triazolo[1,5-c]pyrimidine Derivatives as Highly Potent and Selective Human A<sub>3</sub> Adenosine Receptor Antagonists: Influence of the Chain at the N<sup>8</sup> Pyrazole Nitrogen. *J. Med. Chem.* **2000**, *43*, 4768–4780.
  - (53) Pastorin, G.; Da Ros, T.; Bolcato, C.; Montopoli, C.; Moro, S.; Cacciari, B.; Baraldi, P. G.; Varani, K.; Borea, P. A.; Spalluto, G. Synthesis and Biological Studies of a New Series of 5-Heteroaryl-carbamoylamino-pyrazolo[4,3-e]-1,2,4-triazolo[1,5-c]pyrimidines as Human A<sub>3</sub> Adenosine Receptor Antagonists. Influence of the Heteroaryl Substituent on Binding Affinity and Molecular Modeling Investigation. *J. Med. Chem.* **2006**, *49*, 1720–1729.
  - (54) Karaneswsky, C.; Thomson, D.; Michellys, A.; Ruppar, P.; Chen, J. H. *PCT Int. Appl.* **2005**, WO2005009104200–2005009140716.
  - (55) Klotz, K. N.; Hessling, J.; Hegler, J.; Owman, C.; Kull, B.; Fredholm, B. B.; Lohse, M. J. Comparative Pharmacology of Human Adenosine Receptor Subtypes-Characterization of Stably Transfected Receptors in CHO Cells. *Naunyn-Schmiedeberg's Arch. Pharmacol.* **1998**, *357*, 1–9.
  - (56) De Lean, A.; Hancock, A. A.; Lefkowitz, R. J. Validation and Statistical Analysis of a Computer Modeling Method for Quantitative Analysis of Radioligand Binding Data for Mixtures of Pharmacological Receptor Subtypes. *Mol. Pharmacol.* **1982**, *21*, 5–16.
  - (57) Klotz, K. N.; Cristalli, G.; Grifantini, M.; Vittori, S.; Lohse, M. J. Photoaffinity Labeling of A<sub>1</sub> Adenosine Receptors. *J. Biol. Chem.* **1985**, *260*, 14659–14664.
  - (58) Cheng, Y. C.; Prusoff, H. R. Relationships Between the Inhibition Constant (K<sub>i</sub>) and the Concentration of Inhibitor which Causes 50% Inhibition (IC<sub>50</sub>) of an Enzymatic Reaction. *Biochem. Pharmacol.* **1973**, *22*, 3099–3108.
  - (59) Brown, G.; Wyatt, J.; Harris, R.; Yao, X. Diversity Creation Methods: a Survey and Categorisation. *J. Inf. Fusion* **2005**, *6*, 1–28.
  - (60) Cacciari, B.; Bolcato, C.; Spalluto, G.; Klotz, K.-N.; Bacilieri, M.; Defflorian, F.; Moro, S. Pyrazolo-triazolo-pyrimidines as Adenosine Receptor Antagonists: A Complete Structure-Activity Profile. *Purine Signalling* **2007**, *3*, 183–193.
  - (61) Colotta, V.; Catarzi, D.; Varano, F.; Calabri, F. R.; Lenzi, O.; Filacchioni, G.; Trincavelli, L.; Martini, C.; Defflorian, F.; Moro, S. 1,2,4-Triazolo[4,3-a]quinoxalin-1-one Moiety as an Attractive Scaffold to Develop New Potent and Selective Human A<sub>3</sub> Adenosine Receptor Antagonists: Synthesis, Pharmacological and Ligand-Receptor Modeling Studies. *J. Med. Chem.* **2004**, *47*, 3580–3590.
  - (62) Catarzi, D.; Colotta, V.; Varano, F.; Calabri, F. R.; Lenzi, O.; Filacchioni, G.; Trincavelli, L.; Martini, C.; Tralli, A.; Montopoli, C.; Moro, S. 2-Aryl-8-chloro-1,2,4-triazolo[1,5-a]quinoxalin-4-amines as Highly Potent A<sub>1</sub> and A<sub>3</sub> Adenosine Receptor Antagonists. *Bioorg. Med. Chem.* **2005**, *13*, 705–715.
  - (63) Catarzi, D.; Colotta, V.; Varano, F.; Lenzi, O.; Filacchioni, G.; Trincavelli, L.; Martini, C.; Montopoli, C.; Moro, S. 1,2,4-Triazolo[1,5-a]quinoxaline as a Versatile Tool for the Design of Selective Human A<sub>3</sub> Adenosine Receptor Antagonists: Synthesis, Biological Evaluation and Molecular Modeling Studies of 2-(hetero)aryl- and 2-carboxy-substituted Derivatives. *J. Med. Chem.* **2005**, *48*, 7932–7945.
  - (64) Lenzi, O.; Colotta, V.; Catarzi, D.; Varano, F.; Filacchioni, G.; Martini, C.; Trincavelli, L.; Ciampi, O.; Marighetti, F.; Morizzo, E.; Moro, S.

- 4-Amido-2-aryl-1,2,4-triazolo[4,3-a]quinoxalin-1-ones as New Potent and Selective Human A<sub>3</sub> Adenosine Receptor Antagonists. Synthesis, Pharmacological Evaluation and Ligand-Receptor Modeling Studies. *J. Med. Chem.* **2006**, 49, 3916–3925.
- (65) Moro, S.; Deflorian, F.; Spalluto, G.; Pastorin, G.; Cacciari, B.; Kim, S. K.; Jacobson, K. A. Demystifying the Three Dimensional Structure of G Protein-Coupled Receptors (GPCRs) with the Aid of Molecular Modeling. *Chem. Commun. (Cambridge)* **2003**, 2949–2956.
- (66) Moro, S.; Deflorian, F.; Bacilieri, M.; Spalluto, G. Novel Strategies for the Design of New Potent and Selective Human A<sub>3</sub> Receptor Antagonists: an Update. *Curr. Med. Chem.* **2006**, 13, 639–645.
- (67) Gao, Z. G.; Chen, A.; Barak, D.; Kim, S. K.; Muller, C.; Jacobson, K. A. Identification by Site-Directed Mutagenesis of Residues Involved in Ligand Recognition and Activation of the Human A<sub>3</sub> Adenosine Receptor. *J. Biol. Chem.* **2002**, 277, 19056–19063.

CI700300W